Supporting Information

In vitro and in vivo antiproliferative activity of organo-nickel SCS-pincer complexes on estrogen responsive MCF7 and MC4L2 breast cancer cells. Effect of amine fragments substitutions on the BSA binding and cytotoxicity

Mahboubeh Hosseini-Kharat [a,b,*], Davit Zargarian[a,†], Ali Mohammad Alizadeh[b,c,‡], Kazem Karami[d], Maryam Saeidifar[e], Solmaz Khalighfard[f], Laurent Dubrulle[a], Mostafa Zakariazadeh[g], Jean-Philippe Cloutier[a], Zahra Sohrabijam[e]

[a]*Département de Chimie, Université de Montréal, Montréal, Québec H3C 3J7, Canada*
[b]*Cancer Research Center, Tehran University of Medical Sciences, Tehran, Iran*
[c]*Breast Disease Research Center, Tehran University of Medical Sciences, Tehran, Iran*
[d]*Department of Chemistry, Isfahan University of Technology, Isfahan 84156-83111, Iran*
[e]*Department of Nanotechnology and Advanced Materials, Materials and Energy Research Center, Karaj, Iran*
[f]*Department of Biology, Science and Research Branch, Islamic Azad University, Tehran, Iran*
[g]*Research Institute for Fundamental Sciences (RIFS), University of Tabriz, Tabriz, Iran*

Contents:

* Corresponding author 1: Mahboubeh Hosseini-Kharat (E-mail address: m.hosseinikharat@gmail.com).
† Corresponding author 2: Davit Zargarian (E-mail address: zargarian.davit@umontreal.ca).
‡ Corresponding author 3. Ali Mohammad Alizadeh (E-mail address: aalizadeh@sina.tums.ac.ir).

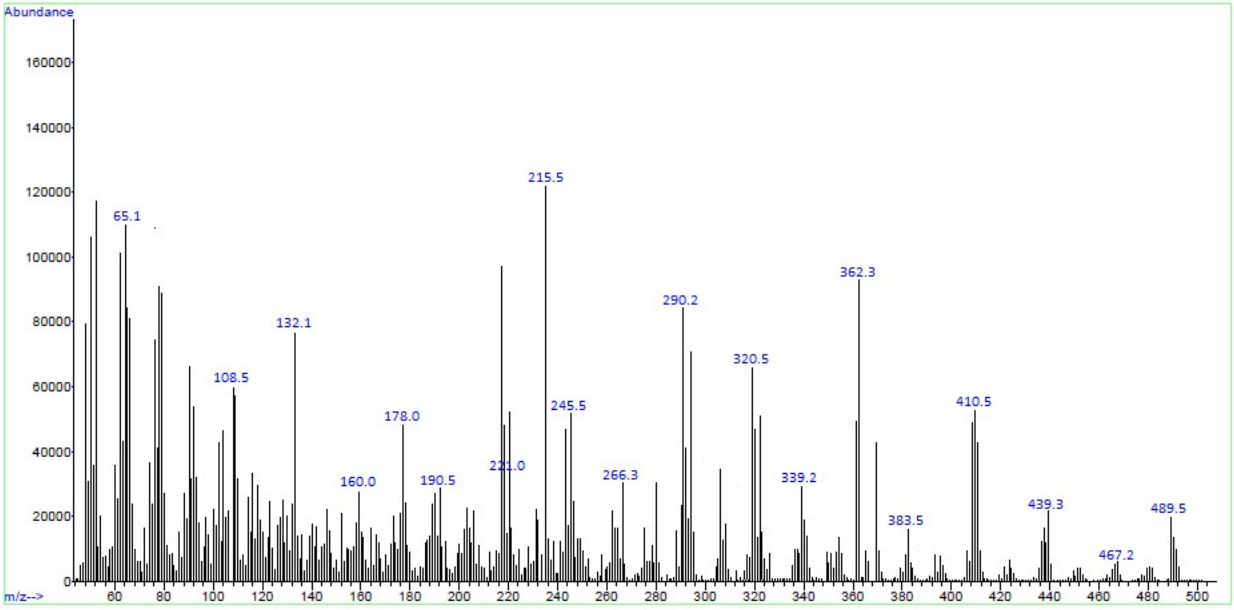
Abundance
m/z-->
65.1
108.5
132.1
160.0
178.0
190.5
215.5
221.0
245.5
266.3
290.2
320.5
339.2
362.3
383.5
410.5
439.3
467.2
489.5

(A)

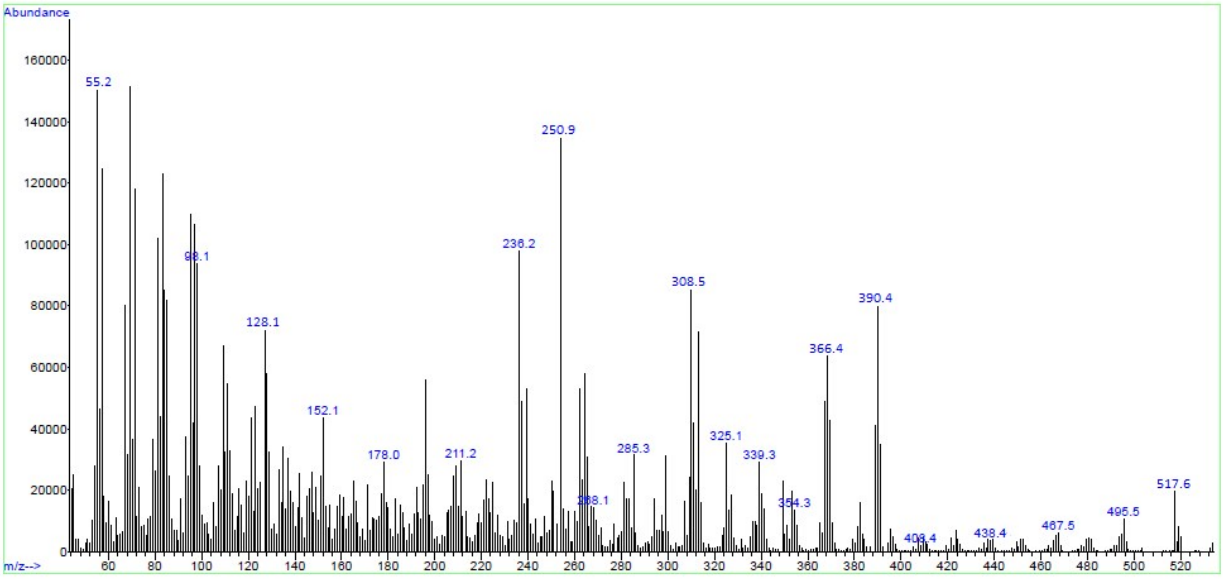
Abundance
m/z-->
55.2
98.1
128.1
152.1
178.0
211.2
236.2
250.9
285.3
308.5
325.1
339.3
366.4
390.4
517.6

(B)

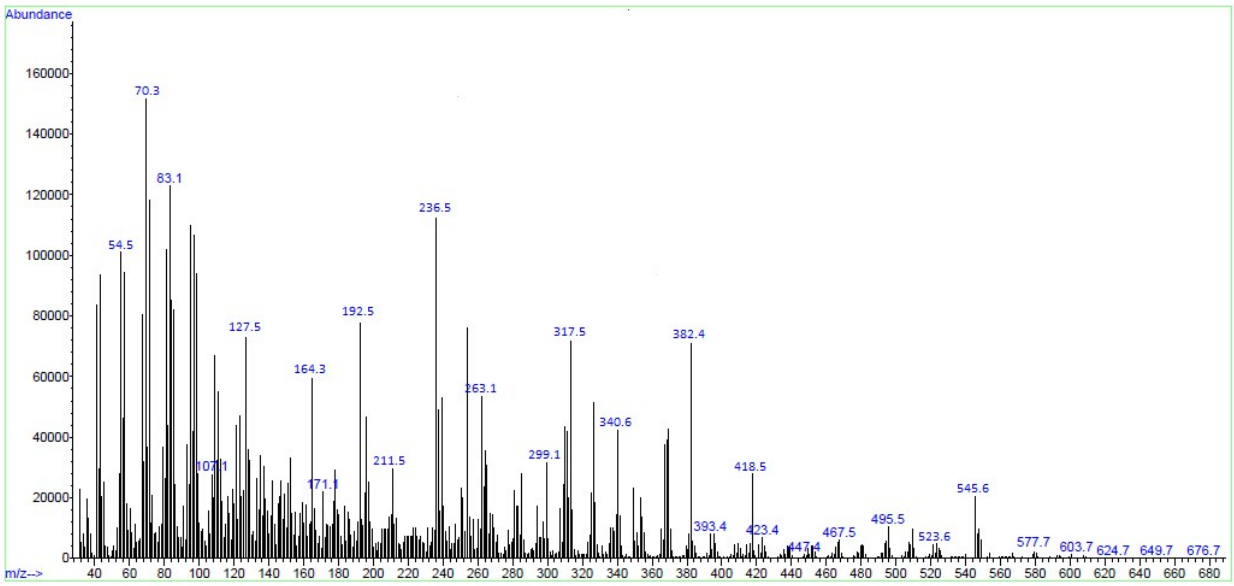

(C)

Figure S1. Mass spectra of **NiL1** (A), **NiL2** (B) and **NiL3** (C).

NiL1

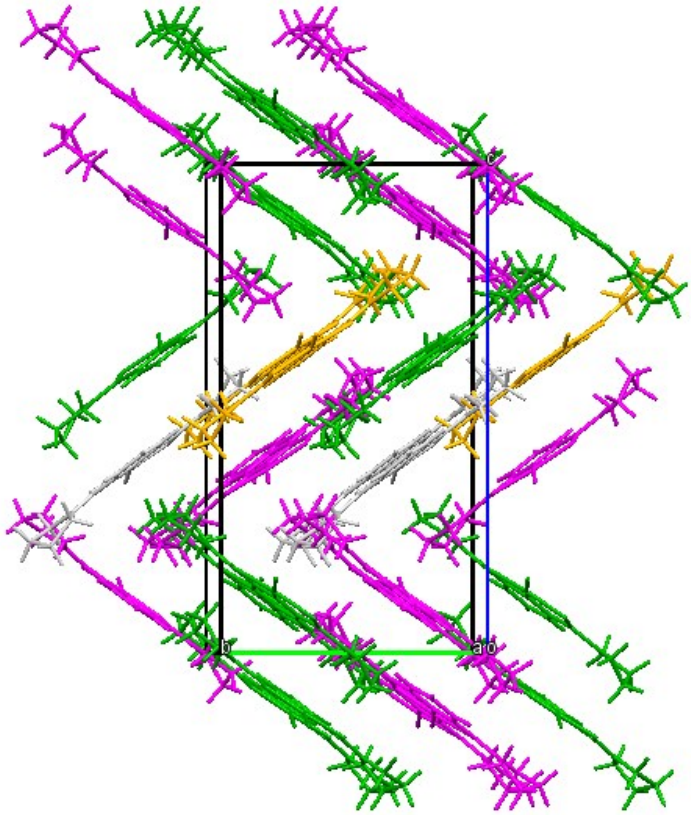

NiL2

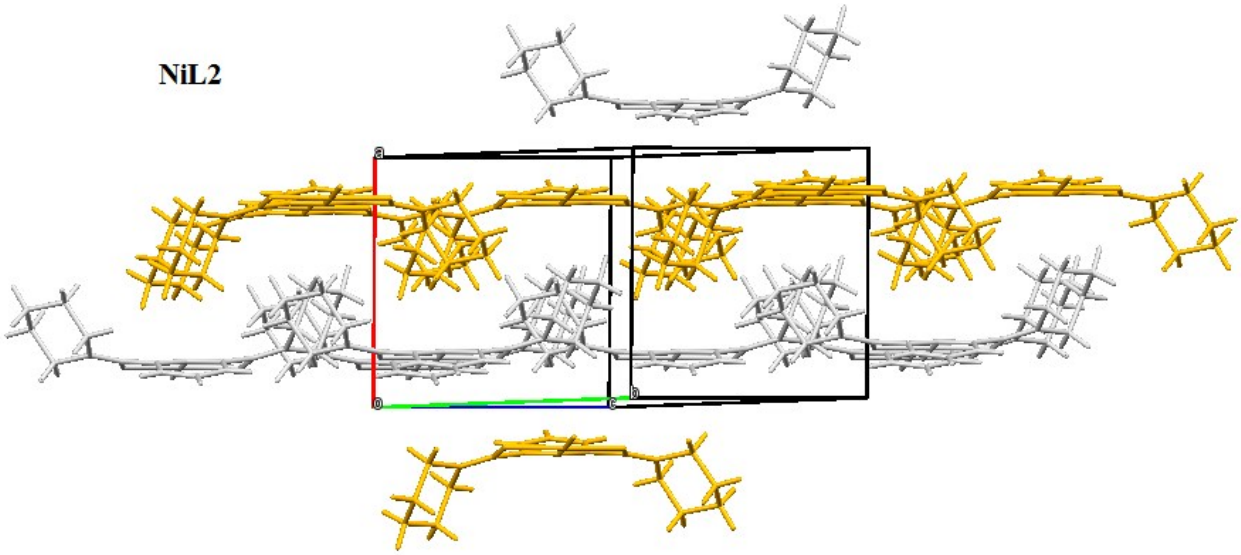

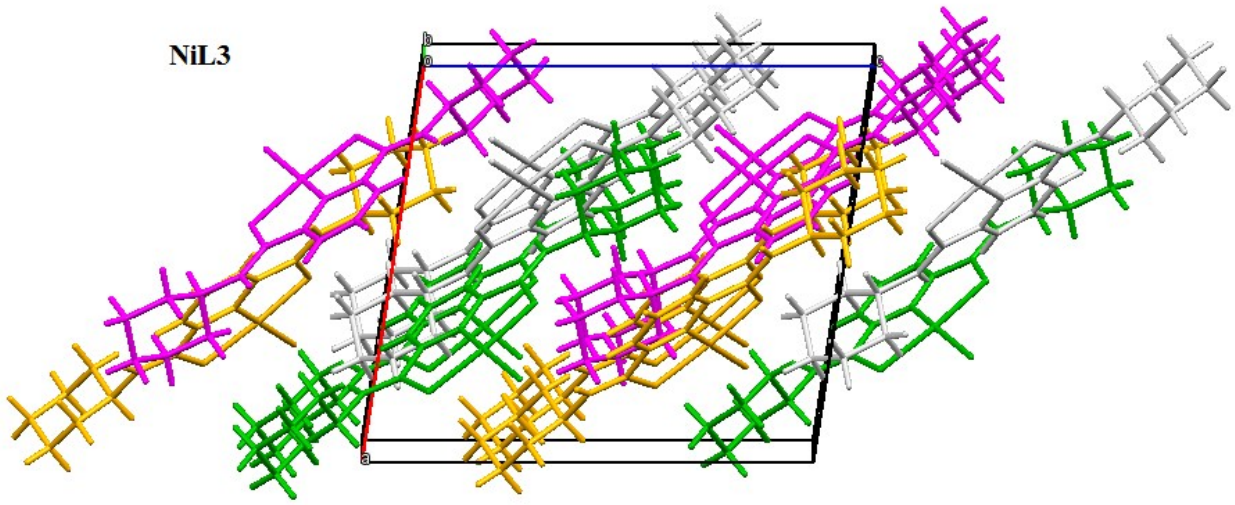

Figure S2. Packing diagrams of **NiL1** (along a axis), **NiL2** (along b axis) and **NiL3** (along b axis). Adjacent molecules connected via CH-π interaction.

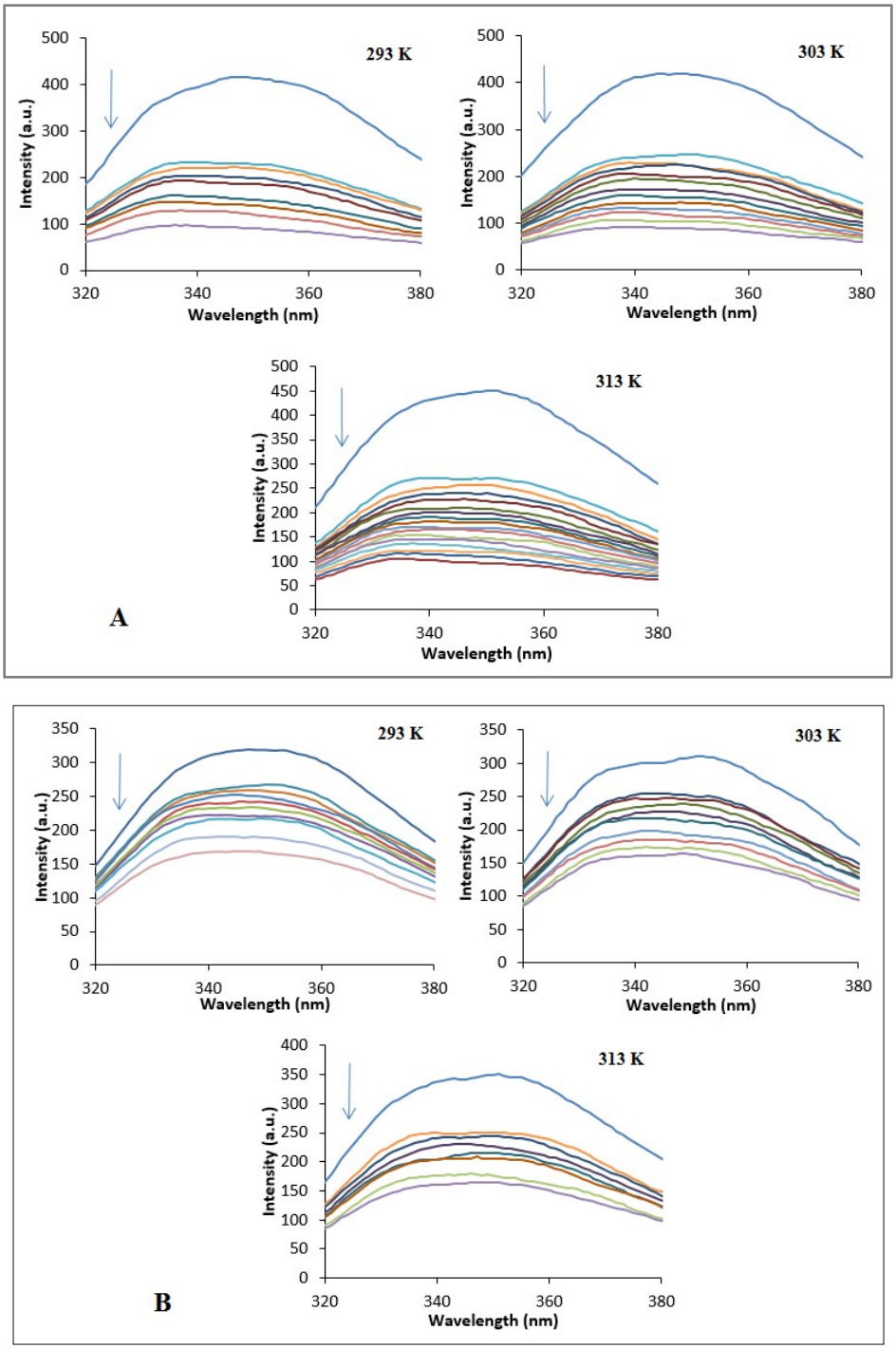

Figure S3. Fluorescence emission spectra of **NiL1**-BSA (A) and **NiL3**-BSA (B) systems at different temperatures. ([BSA] =4.2 μM, [**NiL1**]=0─0.62, [**NiL3**]=0─0.72 mM at Tris–HCl buffer (0.02 M and 0.02 M NaCl), pH 7.4 at 298 K).

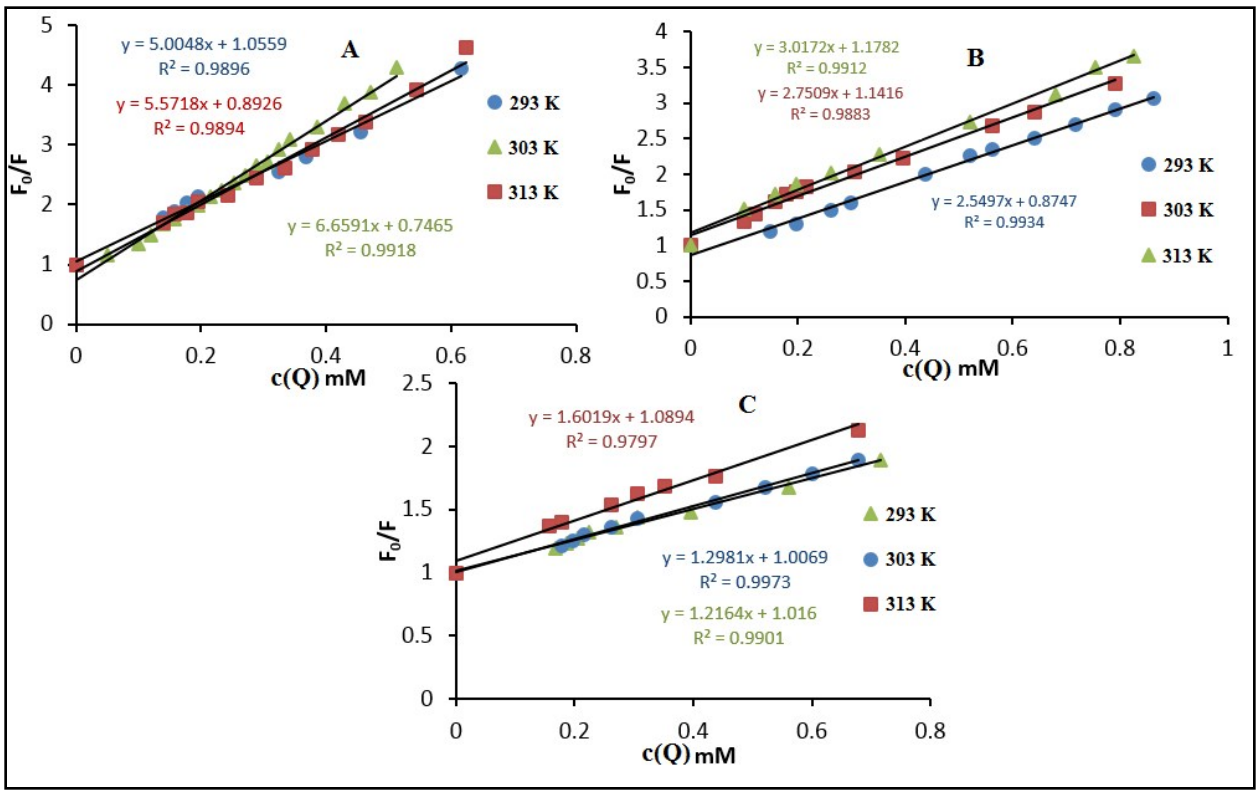

Figure S4. Stern-Volmer plots for **NiL1** + BSA (A), **NiL2** + BSA (B) and **NiL3** + BSA (C) titrations at different temperatures.

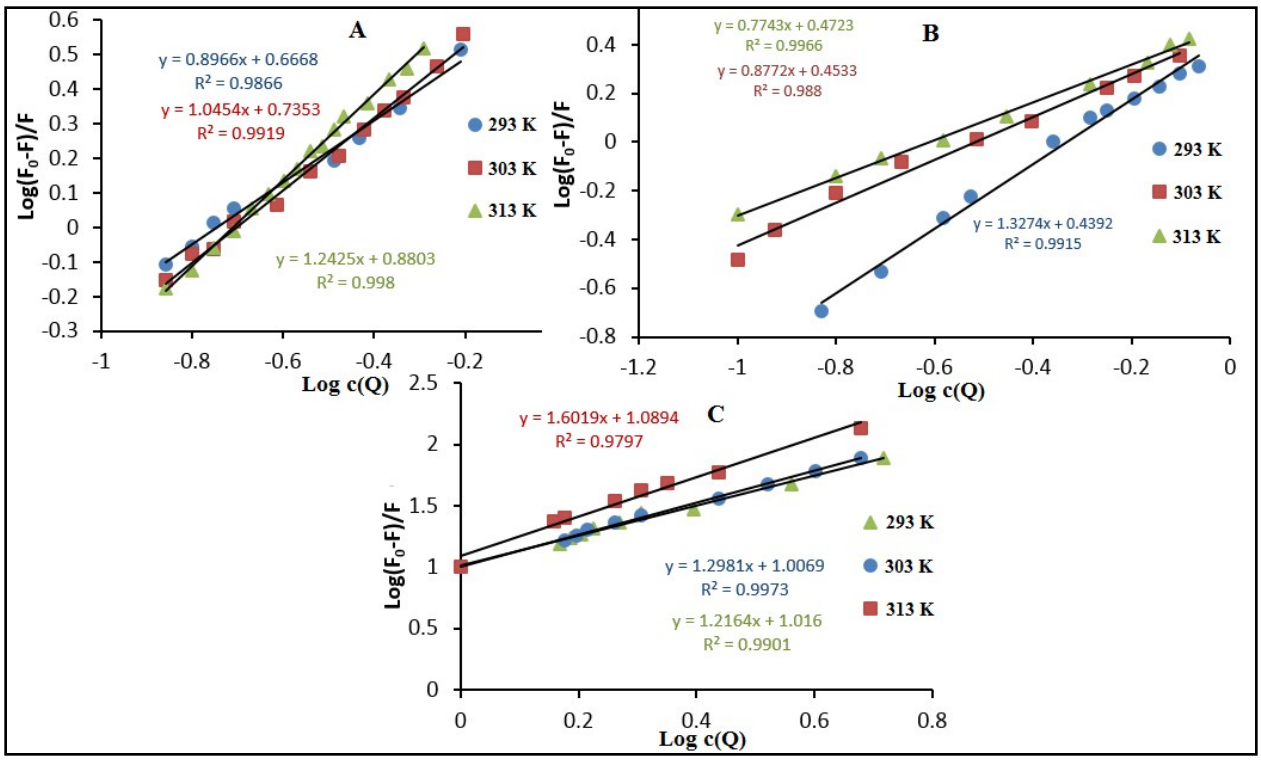

Figure S5. Double-log plots for the fluorescence quenching of the BSA by **NiL1** (A), **NiL2** (B) and **NiL3** (C) at 293, 303 and 313 K.

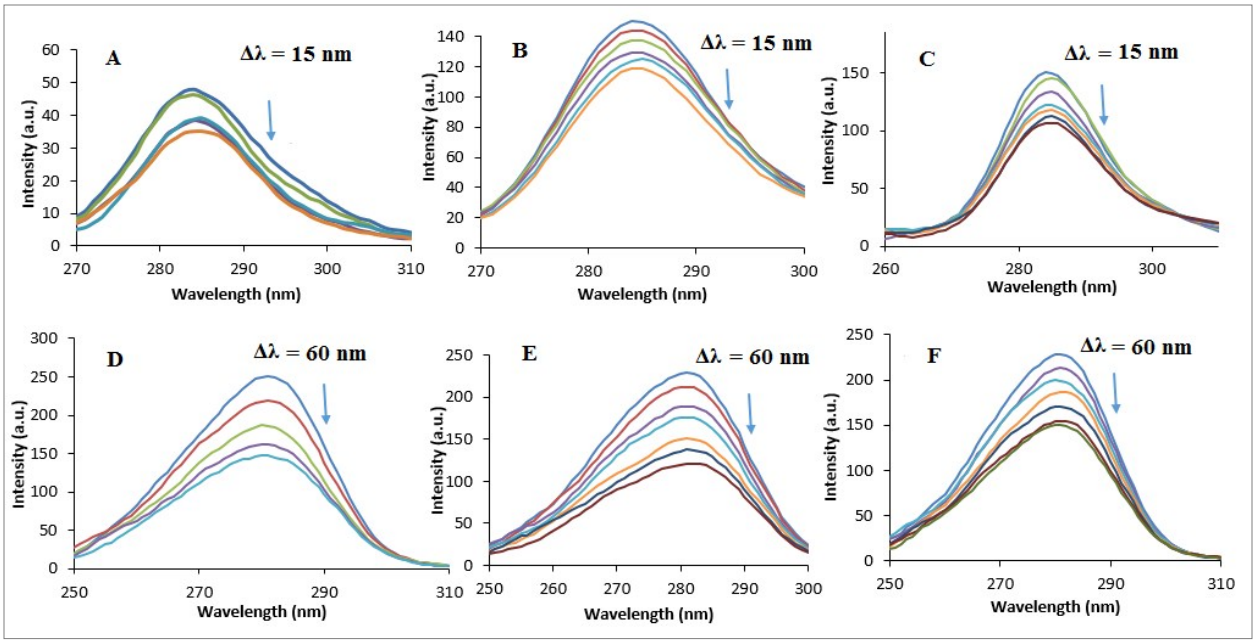

Figure S6. Synchronous fluorescence spectra of BSA (4.2 μM) in the presence of different concentrations of **NiL1** (0─0.24 mM) (A, D), **NiL2** (0─0.24 mM**)** (B, E) and **NiL3** (0─0.24 mM) (C, F) (Δλ= 15 nm and Δλ= 60 nm at Tris–HCl buffer (0.02 M and 0.02 M NaCl), pH 7.4 at 298 K).

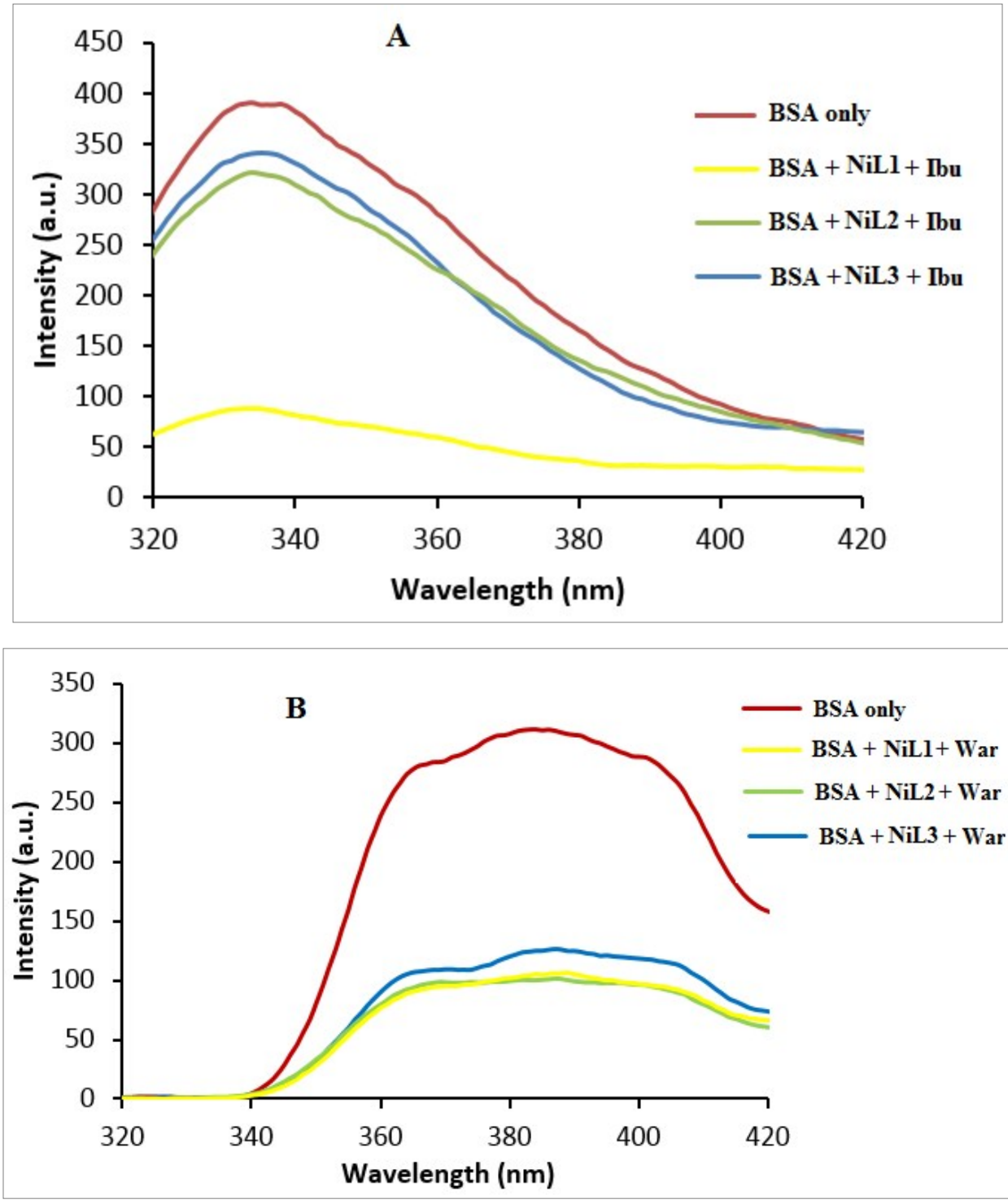

Figure S7. Influence of selected site markers Ibuprofen (0.02 mM) (A) and Warfarin (0.03 mM) (B) on the fluorescence **NiL** bound to BSA.

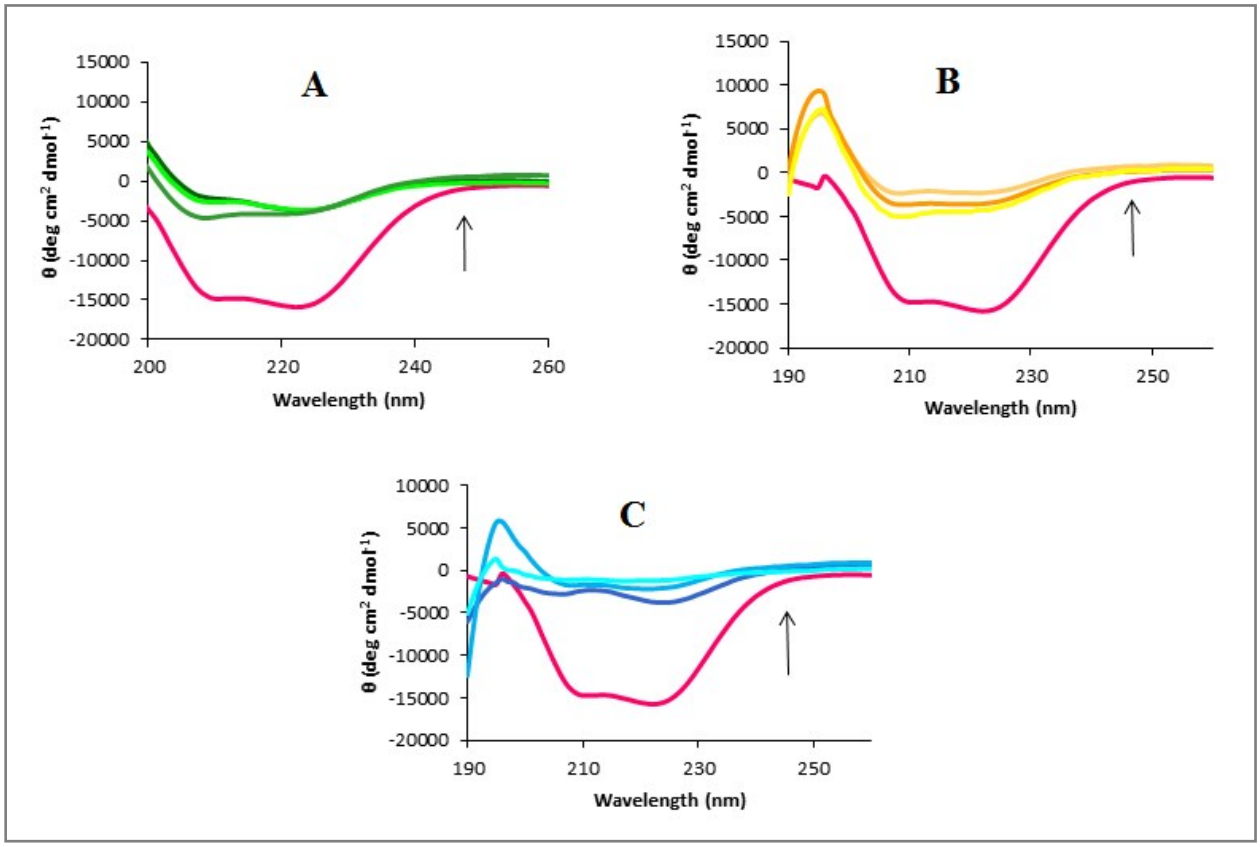

Figure S8. CD of BSA (4.2 μM) in the absence and presence of **NiL1** (A), **NiL2** (B) and **NiL3** (C).

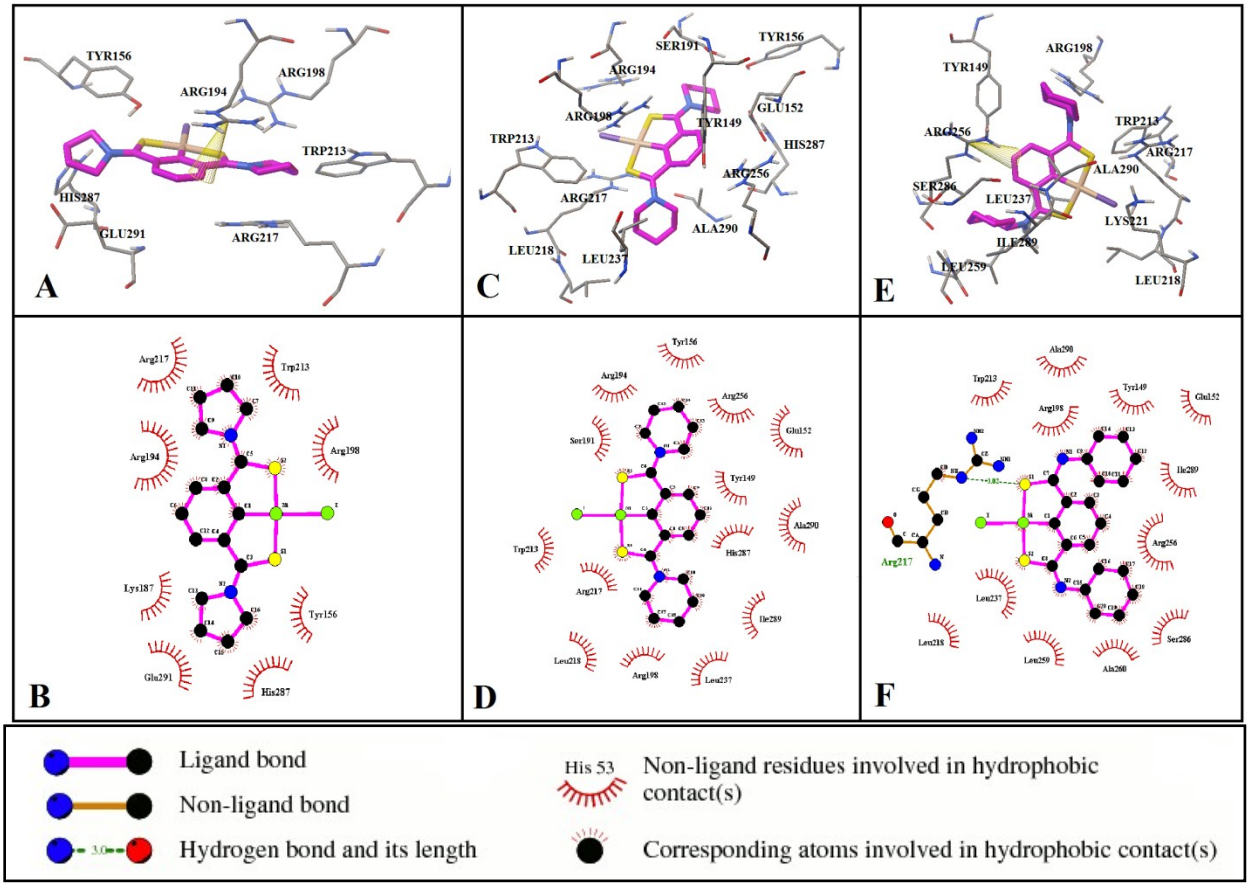

Figure S9. Two- and three-dimensional representation of interactions of nickel pincer complexes with BSA in the Sudlow's site I. H-bonding and cation–π interactions are shown by green dashed lines and mesh structures. **NiL1**-BSA (A,B), **NiL2**-BSA (C,D), **NiL3**-BSA (E,F).

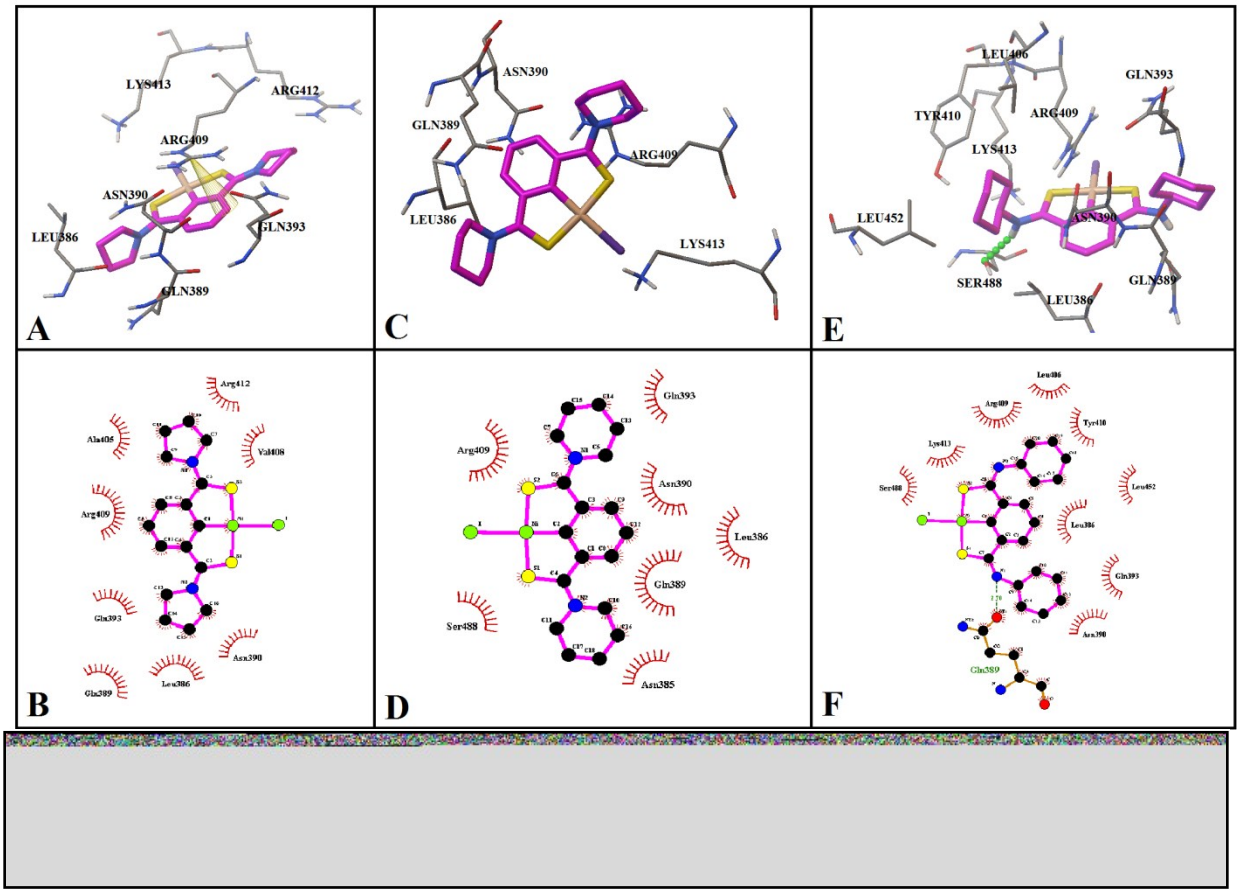

Figure S10. Two- and three-dimensional representation of interactions of nickel pincer complexes with BSA in the Sudlow's site II. H-bonding and cation–π interactions are shown by green spheres and mesh structures. **NiL1**-BSA (A,B), **NiL2**-BSA (C,D), **NiL3**-BSA (E,F).

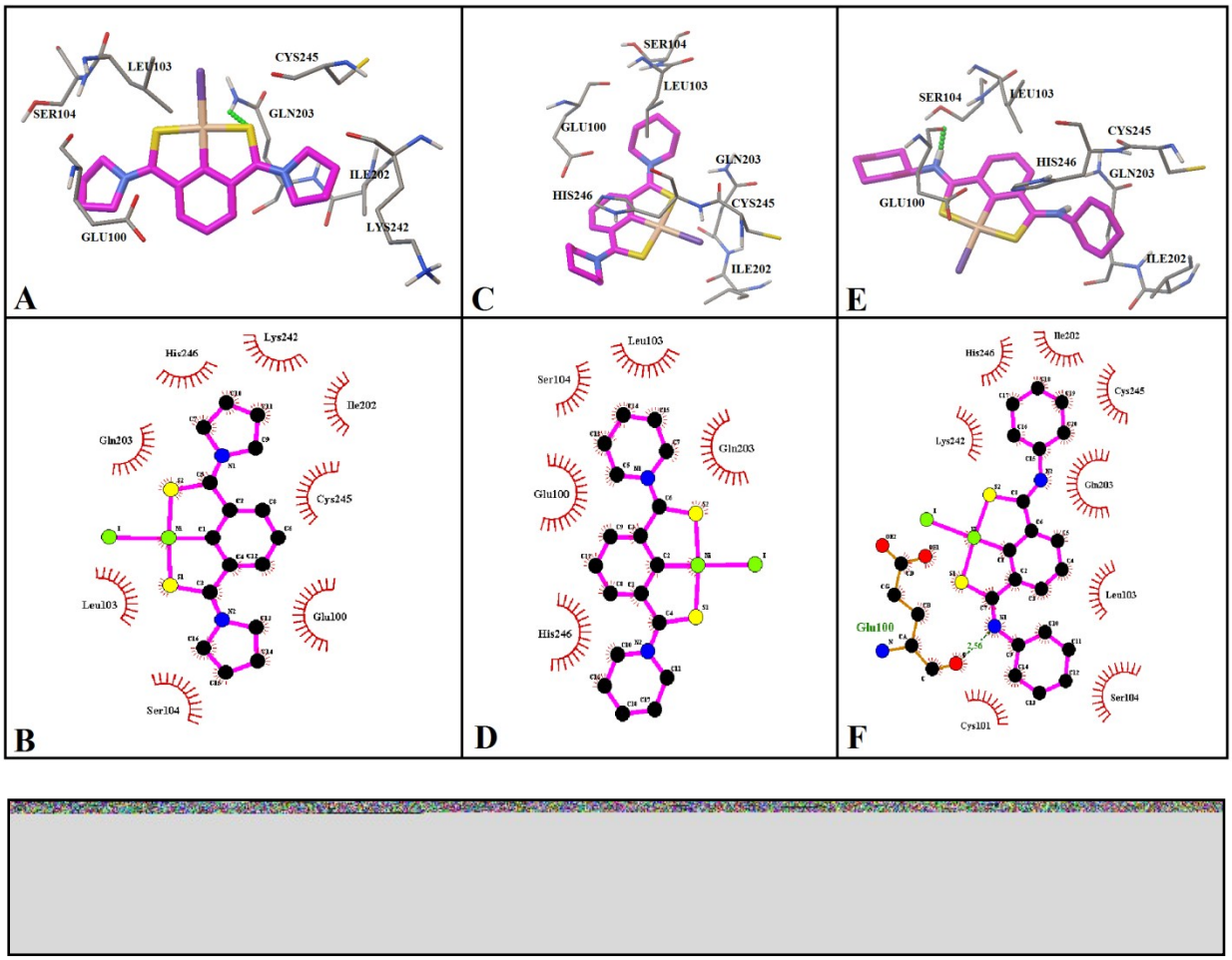

Figure S11. Two- and three-dimensional representation of interactions of nickel pincer complexes with BSA in the MMBS. H-bonding and cation–π interactions are shown by green spheres and mesh structures. **NiL1**-BSA (A,B), **NiL2**-BSA (C,D), **NiL3**-BSA (E,F).

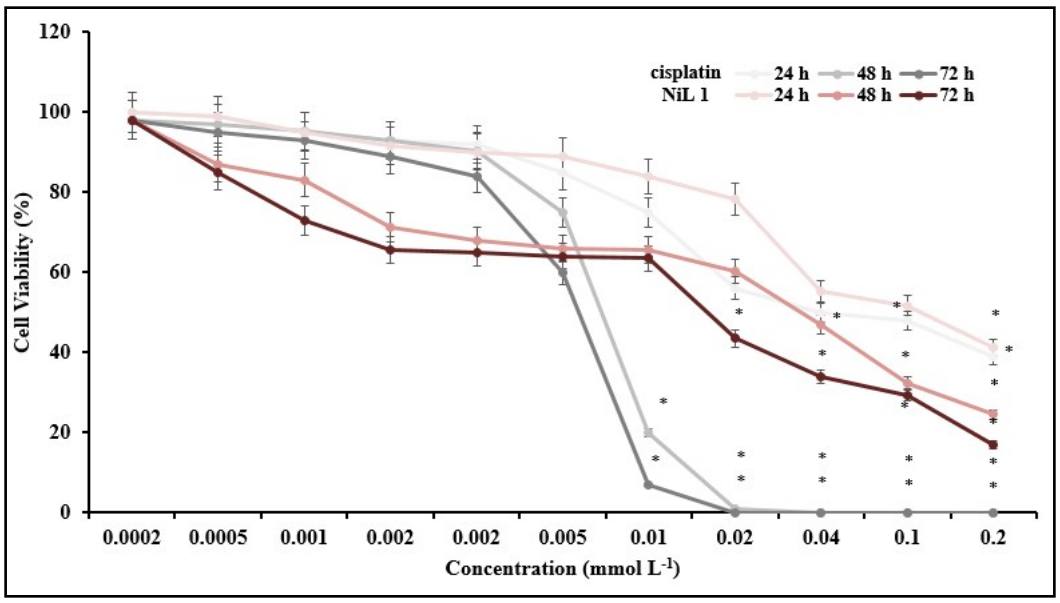
cisplatin
NiL 1
24 h
48 h
72 h
24 h
48 h
72 h
Cell Viability (%)
120
100
80
60
40
20
0
0.0002
0.0005
0.001
0.002
0.002
0.005
0.01
0.02
0.04
0.1
0.2
Concentration (mmol L-1)

(A)

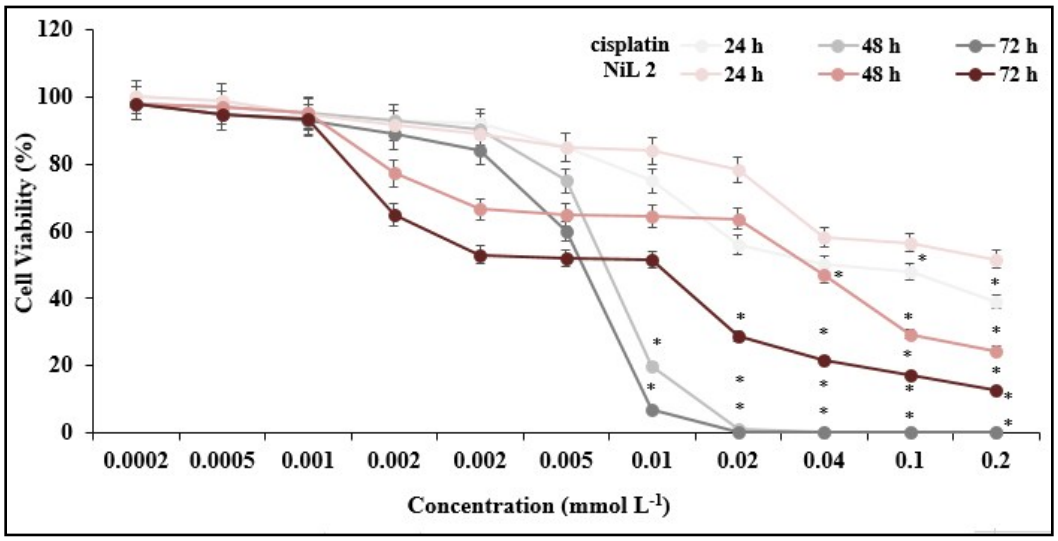
cisplatin
NiL 2
24 h
48 h
72 h
24 h
48 h
72 h
Cell Viability (%)
120
100
80
60
40
20
0
0.0002
0.0005
0.001
0.002
0.002
0.005
0.01
0.02
0.04
0.1
0.2
Concentration (mmol L-1)

(B)

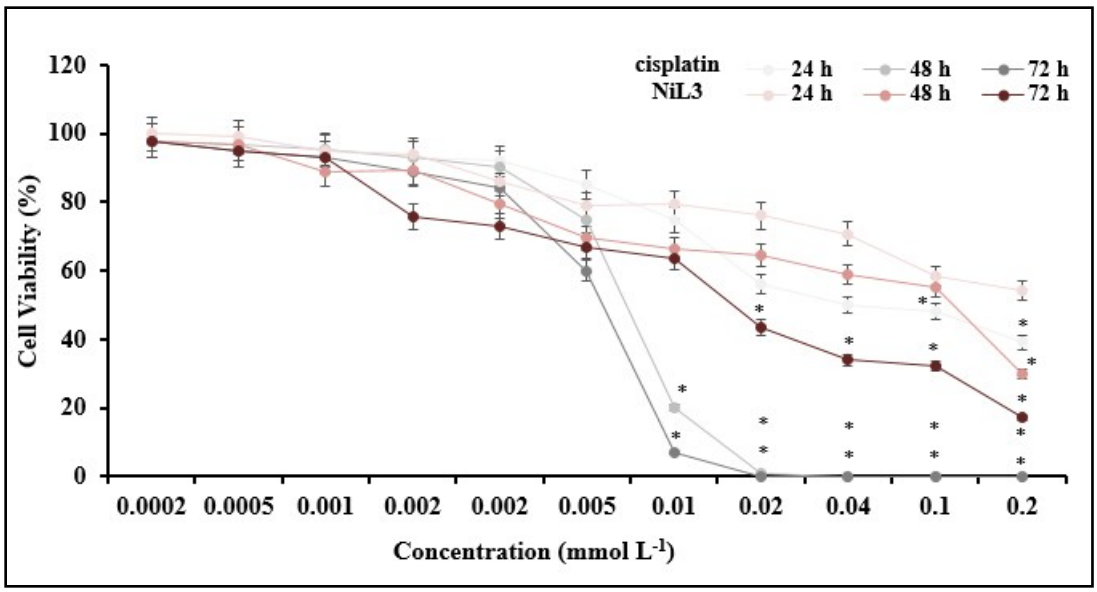

(C)

Figure S12. MCF7 cells were treated with **NiL1** (A), **NiL2** (B), **NiL3** (C) and cisplatin within 24, 48 and 72 h.

Table S1. Selected bond lengths (Å) and bond angles (°) of nickel pincer complexes.

Atoms	**NiL1**	**NiL2**	**NiL3**
Ni1—I1	2.5620 (7)	2.5733 (9)	2.5325 (16)
Ni1—C1	1.874 (5)	1.888 (6)	1.877 (11)
Ni1—S1	2.1431 (12)	2.1638 (18)	2.170 (4)
Ni1—S2	2.1462 (13)	2.1787 (17)	2.153 (4)
C7—S1	1.713 (4)	1.717 (6)	1.722 (12)
C7—N1	1.329 (6)	1.318 (8)	1.316 (14)
C1—C2	1.427 (6)	1.413 (9)	1.413 (15)
C1—C6	1.428 (6)	1.418 (8)	1.415 (15)
S2—Ni1—I1	92.32 (4)	92.76 (5)	91.84 (9)
S1—Ni1—I1	91.91 (4)	92.32 (5)	93.00 (10)
S1—Ni1—S2	174.90 (5)	174.65 (7)	174.94 (13)
C1—Ni1—I1	174.08 (13)	177.2 (2)	175.4 (3)
C1—Ni1—S2	88.12 (14)	87.9 (2)	87.0 (4)
C1—Ni1—S1	87.96 (14)	86.9 (2)	88.3 (4)
C7—S1—Ni1	101.46 (15)	102.0 (2)	100.0 (4)
C2—C1—Ni1	121.3 (3)	121.3 (5)	119.9 (9)
C6—C1—Ni1	120.9 (3)	120.0 (5)	122.0 (9)
C2—C1—C6	117.8 (4)	117.8 (6)	117.9 (10)
C5—C6—C1	120.4 (4)	119.4 (6)	120.5 (12)

Table S2. 3D fluorescence spectral characteristic parameters of Ni-BSA system.

Complex	Peak position	$\lambda_{ex}/\lambda_{em}$	Intensity (F)	F_0/F
NiL1	peak 1	280/343	56.09	4.28
NiL1	peak 2	230/324	42.12	7.06
NiL2	peak 1	280/340	197.92	1.21
NiL2	peak 2	230/345	170.14	1.75
NiL3	peak 1	280/343	203.03	1.18
NiL3	peak 2	230/338	130.25	2.28

Table S3. Calculated bond lengths of the non-covalent interactions in binding of nickel complexes to different binding sites of BSA.

Studied binding sites of BSA	Interacting residues	Non-covalent interactions	Distance (Å)
Sudlow's site I	**NiL1**-BSA:ARG194:CZ	cation-π interaction	4.1
Sudlow's site I	**NiL3**-BSA:ARG256:CZ	cation-π interaction	4.9
Sudlow's site II	**NiL1**-BSA:ARG409:CZ	cation-π interaction	3.9
Sudlow's site II	**NiL3**-H-BSA:SER488:OG	H-bonding	1.9
NTS	**NiL1**-BSA:HIS3	π–π stacking interaction	5.1
NTS	**NiL1**-BSA:HIS9	π–π stacking interaction	5.4
NTS	**NiL2**-BSA:HIS3	π–π stacking interactions	4.4
NTS	**NiL2**-BSA:HIS9	π–π stacking interaction	3.8
NTS	**NiL3**-H-BSA:ASP1:O	H-bonding	1.8
NTS	**NiL3**-S-BSA:THR2:HG	H-bonding	2.2
MMBS	**NiL1**-S-BSA:GLN203:HE	H-bonding	2.2
MMBS	**NiL3**-H-BSA:GLU100:O	H-bonding	1.9

Table S4. Determination of IC_{50} (mM) values of **NiL** in MCF7 cells after 24, 48 and 72 h incubation.

	IC50 (mM)		
Compound	24 h	48 h	72 h
NiL1	0.1	0.04	0.02
NiL2	> 0.2	0.04	0.02
NiL3	> 0.2	0.2	0.02
Cisplatin	0.04	0.01	0.01

Experimental section

Crystal Structure Determinations

Suitable crystals of **NiL** for X-Ray crystallography were obtained via diffusion of diethyl ether into the DMSO solution of these compounds. The crystallographic data for **NiL** were collected from a single crystal sample which was mounted on a loop fiber. Data were collected using a Bruker Venture diffractometer equipped with a photon 100 CMOS Detector, a Helios MX optics and a Kappa goniometer. The crystal-to-detector distance was 4.0 cm, and the data collection was carried out in 1024 × 1024 pixel mode. Cell refinement and data reduction were done using SAINT [1]. An empirical absorption correction, based on the multiple measurements of equivalent reflections, was applied using the program SADABS [2]. The space group was confirmed by XPREP routine [3] in the program SHELXTL [4]. The structures were solved by direct methods and refined by full matrix least-squares and difference Fourier techniques with SHELX-97 [5,6]. All non-hydrogen atoms were refined with anisotropic displacement parameters, while hydrogen atoms were set in calculated positions and refined as riding atoms with a common thermal parameter.

BSA binding studies

BSA solutions was prepared by dissolving appropriate amounts of solid BSA in buffer tris(hydroxymethyl)aminomethane in sodium chloride (Tris–HCl) 0.02 M, 0.02 M NaCl, pH 7.4. The concentration of BSA was determined spectrophotometrically using the extinction coefficient of 43,300 $M^{-1}cm^{-1}$ at 280 nm [7]. The stock solution of nickel complexes (10^{-3} M) was prepared by dissolving appropriate amounts of **NiL** in Tris–HCl buffer.

To investigate the stability of compounds in biological media, (Tris-HCl) 0.02 M, 0.02 M NaCl (pH 7.4) was added to the aqueous and DMSO solutions of the Ni(II) complexes, and the resulting solutions were allowed to stand for 10 days. UV-Vis spectra of the aged solutions showed no change in the absorption of the three compounds. Furthermore, the pH of the solutions remained constant, showing no evidence of decomposition in the buffer media.

Fluorescence measurements were carried out maintaining a fixed BSA concentration (4.2 μM) in a quartz cell while varying the concentrations of the nickel complexes: 0─0.62 mM (**NiL1**), 0─0.86 mM (**NiL2**) and 0─0.72 mM (**NiL3**) at Tris–HCl buffer (0.02 M and 0.02 M NaCl), pH 7.4. An excitation wavelength of 290 nm was selected and the emission wavelength was recorded from 310 to 500 nm, with both excitation and emission bandwidths set on 5 nm at 293, 303 and 313 K, respectively. The synchronous fluorescence spectra were measured in wavelength ranges from 265 nm to 320 nm for $\Delta\lambda = 15$ nm and from 240 nm to 310 nm for $\Delta\lambda = 60$ nm upon excitation at 290 nm. Into the quartz cell containing the BSA solution (4.2 μM) was titrated the nickel complexes (0─0.24 mM) at Tris–HCl buffer (0.02 M and 0.02 M NaCl), pH 7.4 at 298 K. Three-dimensional fluorescence spectra of BSA in the absence and presence of **NiL1** (0.1 mM) were measured under the following conditions: the emission wavelength was recorded between 200 and 500 nm, the initial excitation wavelength was set at 200 nm with an increment of 5 nm, and the other scanning parameters were the same as those for the fluorescence emission spectra (Tris–HCl buffer (0.02 M and 0.02 M NaCl), pH 7.4 at 298 K). The circular dichroism (CD) spectra of BSA in the presence of nickel complexes were recorded in the range of 190–260 nm and bandwidth 1 nm at 298 K under constant nitrogen flush. The molar ratio of **NiL** to BSA was varied (1.19, 2.38 and 4.76) and each CD spectrum was the average of three successive scans. The contents of

different secondary structures of BSA were analyzed by using CDNN software equipped with the spectrometer.

Molecular docking approach

AutoDock 4.2.6 using Lamarckian genetic algorithm together with the AutoDock Tools 1.5.6 was employed to set up and perform docking calculations of the nickel complexes binding to BSA [8]. Three-dimensional chemical structures of studied complexes have been provided by converting the crystallographic CIF files to the PDB files via Open Babel 2.3.2 software [9]. The PDB ID code: 4F5S (chain A) with 2.47Å resolution has been selected from the RCSB protein data bank *(http://www.pdb.org)* for BSA structure. During target protein preparation, the heteroatoms including water molecules were deleted and polar hydrogen atoms and Kollman charges were added to the receptor molecule (BSA).

For docking simulation in this study, four different possible binding sites on BSA structure for interaction with nickel complexes were considered independently. These binding sites included Sudlow's sites I and II as common drug binding sites on BSA, as well as the metal binding N-terminal site (NTS) and multi-metal binding site (MMBS) [10–12]. In the docking analysis, the binding sites were assigned to four possible mentioned binding sites on BSA, which were enclosed in boxes with number of grid points in x × y × z directions, 50 × 50 × 50 $Å^3$ (for Sudlow's sites I and II) 50 × 40 × 50 $Å^3$ (for NTS binding site) and 50 × 60 × 50 $Å^3$ (for MMBS) with grid spacing of 0.375 Å for all boxes. Visualization of the docked poses have been done by using PyMOL. The schematic two-dimensional diagram of molecular interactions between complexes and BSA prepared by LIGPLOT$^+$ v1.4.4 software [13].

MTT assay

The MTT [3-(4,5-dimethylthiazol-2-yl)-2,5-diphenyl-tetrazolium bromide] colorimetric assay [14] was used to investigate the cytotoxicity of the nickel pincer complexes, **NiL**. This test is based on the metabolic reduction of soluble MTT by mitochondrial enzyme activity of viable tumor cells. The product is an insoluble, colored formazan that can be quantified spectrophotometrically after dissolution in DMSO. Human breast cancer cell line MCF7 was supplied from the National Cell Bank of Pasture Institute, Tehran, Iran. MCF7 cells were cultured in Dulbecco's Modified Eagle Medium (DMEM) supplemented with 10% heat-inactivated fetal bovine serum (FBS), 100 U mL^{-1} penicillin, 100 µg mL^{-1} streptomycin and 5 mM L-glutamine. Subsequently, the cell lines were grown at 37 ºC in a humidified atmosphere containing 5% CO_2. All reagents and cell culture media were purchased from Gibco Company (Germany). MTT assay was performed on the 50% confluent cells cultivated in 96-well plates (at a seeding density of 1×10^6 cells/well). The cells were exposed to a designated amount of the **NiL**, and incubated at 37 ºC for 2 h. Then, the medium was removed and replaced with fresh medium, and the cells were again incubated at 37 ºC for a designated period of time (24, 48 and 72 h). Finally, 200 µL of MTT (5 mg/mL) was introduced to each well, and the plates were incubated at 37 ºC for 4 h and replaced with 200 µL of DMSO. Relative cell viability was determined using a 96-well plate reader (TECAN, Switzerland) at 570 nm. Measurements were performed and the required concentration for a 50% inhibition of viability (IC_{50}) was determined by graphically standard graph which was plotted by taking the concentration of the drug in X-axis and relative cell viability in the Y-axis [15]. The percentage of viability was calculated by equation 1 wherein OD is optical density.

$$Cell\ viability\ (\%) = \frac{OD(the\ experimental\ group)}{OD\ (control)} \times 100\%$$

Animals

All in vivo experiments were confirmed by the international guidelines of the Weatherall report and Institutional Animal Care and Use Committee (IACUC) of Tehran University of Medical Sciences. All 6-8 old inbred BALB/c mice, obtained from Iran Pasteur Institute, were maintained in large group houses under 12 h dark and light cycles and were provided with food and watered libitum.

Tumor transplantation

MC4L2 cell line was provided from the National Cell Bank of Pasture Institute, Tehran, Iran. MC4L2 cells were grown into solid tumor in female BALB/c mice flank. MC4L2 tumor from the mice bearing breast cancer was cut into pieces below 0.2–0.3 mm^3 and subcutaneously transplanted into mice right flank under anesthesia using 100 mg kg^{-1}, i.p ketamine and 10 mg kg^{-1}, i.p xylazine. The tumors were visible two weeks after tumor implantation [16].

*Therapeutic effects of **NiL1** on a mouse model of breast cancer*

Twenty four mice with breast cancer were randomly divided into three different groups: (1) control, (2) treated with 2 mg kg^{-1} **NiL1** and (3) treated with 10 mg kg^{-1} of **NiL1**. Two weeks post tumor implantation, **NiL1** was intraperitoneally injected for 14 days from day 14 up to day 28. Furthermore, normal saline was given in the control animals. Using a digital vernier caliper (Mitutoyo, Japan), tumor volume was measured two times a week and reported by the equation 2 wherein V is volume, L is length, W is width, and D is depth [17].

$$V = \frac{1}{6(\pi LWD)}$$

Depiction of tumors and metastases

The mice under study were closely monitored for general health during the study period. They were weighed once a week, and observed for evidence of complications and death. Moribund mice were euthanized. The rest were euthanatized at the end of the 4^{th} week. A thorough necropsy was

then performed, and the vital organs including liver, spleen, lung, brain, and bone were examined for lesions and metastatic deposits.

References

[1] SAINT, Release 6.06; Integration Software for Single Crystal Data; Bruker AXS Inc.: Madison, WI, 1999.

[2] G. M. Sheldrick, SADABS, Bruker Area Detector Absorption Corrections; Bruker AXS Inc., Madison, WI, 1999.

[3] XPREP, Release 5.10; X-ray Data Preparation and Reciprocal Space Exploration Program; Bruker AXS Inc.: Madison, WI, 1997.

[4] SHELXTL, Release 5.10; The Complete Software Package for Single Crystal Structure Determination; Bruker AXS Inc.: Madison, WI, 1997.

[5] G. M. Sheldrick, SHELXS97, Program for the Solution of Crystal Structures; Univ. of Gottingen: Germany, 1997.

[6] G. M. Sheldrick, SHELXL97, Program for the Refinement of Crystal Structures; University of Gottingen: Germany, 1997.

[7] I. Goncharova, S. Orlov, M. Urbanova, Biophys. Chem. 180-181 (2013) 55–65.

[8] G.M. Morris, R. Huey, W. Lindstrom, M.F. Sanner, R.K. Belew, D.S. Goodsell, A.J. Olson, J. Comput. Chem. 30 (2009) 2785–2791.

[9] N.M. O'Boyle, M. Banck, C.A. James, C. Morley, T. Vandermeersch, G.R. Hutchison, J. Cheminform. 3:33 (2011).

[10] G. Sudlow, D. J. Birkett, D. N. Wade, Mol Pharmacol., 12 (6) (1976) 1052–1061.

[11] C Harford, B Sarkar, Acc. Chem. Res.,(1997) 123–130.

[12] W. Bal, J. Christodoulou, P.J. Sadler, A. Tucker, J. Inorg. Biochem., 70 (1998) 33–39.

[13] A. C. Wallace, R. A. Laskowski, J. M. Thornton, Protein Eng., 8(2) (1995) 127–134.

[14] C. M. Hackl, B. Schoenhacker-Alte, M. H. M. Klose, H. Henke, M. S. Legina, M. A. Jakupec, W. Berger, B. K. Keppler, O. Brüggemann, I. Teasdale, P. Heffeter, W. Kandioller, Dalton Trans., 46 (2017) 12114–12124.

[15] M. Johari-Ahar, J. Barar, A. M. Alizadeh, S. Davaran, Y. Omidi, M. R. Rashidi, J. Drug Target., 24 (2016) 120–133.

[16] B. Farhangi, M. Latifpour, A. M. Alizadeh, H. Khodayari, S. Khodayari, M. Khaniki, S. Ghasempour, Eur. J. Pharmacol., 765 (2015) 171–178.

[17] A. Isanejad, A. M. Alizadeh, S. A. Shalamzari, H. Khodayari, S. Khodayari, V. Khori, N. Khojastehnjad,. Life Sci., 151 (2016) 30–40.